Layer-by-Layer Evolution of Structure, Strain, and Activity for the Oxygen Evolution Reaction in Graphene-Templated Pt Monolayers

Ali Abdelhafiz,[†] Adam Vitale,[†] Corey Joiner, Eric Vogel, and Faisal M. Alamgir*

School of Materials Science and Engineering, Georgia Institute of Technology, 771 Ferst Drive, Atlanta, Georgia 30332, United States

S *Supporting Information*

ABSTRACT: In this study, we explore the dimensional aspect of structure-driven surface properties of metal monolayers grown on a graphene/Au template. Here, surface limited redox replacement (SLRR) is used to provide precise layer-by-layer growth of Pt monolayers on graphene. We find that after a few iterations of SLRR, fully wetted 4−5 monolayer Pt films can be grown on graphene. Incorporating graphene at the Pt−Au interface modifies the growth mechanism, charge transfers, equilibrium interatomic distances, and associated strain of the synthesized Pt monolayers. We find that a single layer of sandwiched graphene is able to induce a 3.5% compressive strain on the Pt adlayer grown on it, and as a result, catalytic activity is increased due to a greater areal density of the Pt layers beyond face-centered-cubic close packing. At the same time, the sandwiched graphene does not obstruct vicinity effects of near-surface electron exchange between the substrate Au and adlayers Pt. X-ray photoelectron spectroscopy (XPS) and extended X-ray absorption fine structure (EXAFS) techniques are used to examine charge mediation across the Pt-graphene-Au junction and the local atomic arrangement as a function of the Pt adlayer dimension. Cyclic voltammetry (CV) and the oxygen reduction reaction (ORR) are used as probes to examine the electrochemically active area of Pt monolayers and catalyst activity, respectively. Results show that the inserted graphene monolayer results in increased activity for the Pt due to a graphene-induced compressive strain, as well as a higher resistance against loss of the catalytically active Pt surface.

KEYWORDS: *platinum, monolayer, graphene, catalysis, oxygen reduction reaction, X-ray photoelectron spectroscopy, X-ray absorption spectroscopy, cyclic voltammetry*
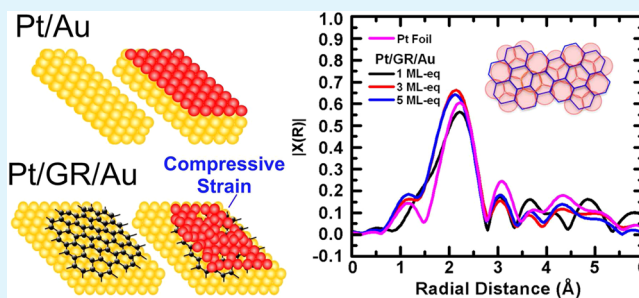
INTRODUCTION

Graphene, with its unique structure and electronic configuration, has become a choice material for incorporation into high performance devices.[1] The inherent advantage of graphene for many applications is not only limited to its mechanical strength, chemical stability, and super aromatic electrical conductivity through its 2D planar structure but is also due to the versatile tuning of electronic structure at the graphene−metal interface, where the insertion of graphene is believed to tune the electronic structure of the whole junction.[2,3] In the area of catalysis, sandwiched single graphene sheets can potentially transform the catalyst/support architecture by introducing singularities in the interface stress and electronic structure. Early studies testing this concept, for example, have been carried out in electrocatalysts to enhance activity for methanol oxidation reaction (MOR).[4] Induced strain along the catalyst surface caused by the insertion of graphene holds the potential to induce surface electrons to more readily catalyze such reactions.[5]

Platinum, as one of the most active catalyst metals, still suffers from high cost and loss of electrochemically active area (ECA) due to dissolution during operation. Incorporation of graphene as a catalyst support for Pt has already shown improvements for boosted catalyst activity and lifetime.[6−8] Li et

al. showed increased catalytic activity of Pt/graphene (Pt/GR) nanocomposites toward the methanol oxidation reaction (MOR) compared to those of Pt/vulcan carbon.[8] Shang et al. demonstrated increased durability of Pt/GR(nanoflakes) compared to Pt/carbon-nanotubes during MOR.[9] While these studies clearly show the benefits of Pt/GR/support architectures, they do not delineate between the effects of structure (dimension and morphology), strain, and charge transfers in improving the catalyst performance. Indeed, through a properly tuned architecture, we posit that the single sandwiched layer of graphene will simultaneously impose strain on the overlayer Pt and allow charge transfers between the Pt and the underlying support (ligand effect). In this paper we systematically investigate the simultaneous strain and charge transfer effects in Pt/GR/Au systems by varying the Pt overlayer coverage one monolayer at a time. We choose Au as the support since it shares a crystal structure with Pt and because the Pt−Au bimetallic system has attracted research interest due to certain synergistic effects. For example, shifts of the d band centers of the core and shell metals allow for better activity with reactions
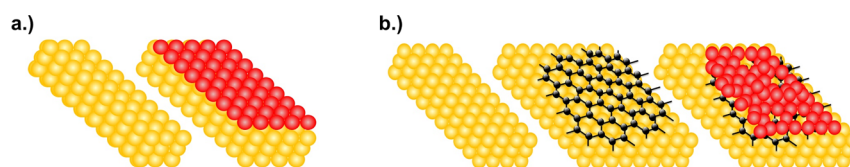
Figure 1. (a) Pt/Au samples, where Pt is grown directly on a bare Au substrate by SLRR. (b) Pt/GR/Au samples, where graphene is first transferred on top of the Au substrate before Pt deposition by SLRR.

such as the ORR, while others showed that for CO oxidation, the initial adlayers of Pt on Au exhibit stronger Pt–CO bonds than bulk Pt.[10,11]

Experimental and computation research on the growth (and the resulting properties) of various metals over graphene, was reviewed by Liu et al. The review summarized many metal systems, but most showed a similar tendency to cluster over graphene.[12] Dai et al. used first-principles energy calculations to investigate the formation and structures of Pt clusters on graphene. Their calculation found that, for a single Pt atom absorption, the most stable absorption site is the bridge site, and that it will preferentially form tetrahedral clusters.[13] Similarly, Chan et al. found through calculation that metals comparable to Pt, such as Pd and Au, induce a noticeable distortion of the graphene sheet upon adsorption.[14] He et al. synthesized Pt, Pd, Au, and Ag nanoparticles onto graphene oxide nanosheets by a solution-based method but was not able to achieve full coverage due to agglomerates.[15] Sun et al. found that depositing Pt nanoparticles via atomic layer deposition (ALD) methods tended to form clusters rather than wetted layers spread over the graphene.[16] Achieving full metal wetting of graphene-based support at monolayer level thickness remains a challenge.

Monolayer (ML) level Pt shells as a part of "core–shell" catalysts have been developed by various groups.[17,18] While ML levels of shell thickness allow catalytically relevant charge transfers from the core, ML Pt can exhibit weak chemical stability and unevolved metallic bonding.[19,20] For our systematic study of the dimensional dependence of structure and property evolution, highly wetted and precisely controlled deposition of Pt MLs is critical. To address this challenge we employ a self-limiting electrodeposition method that is thermodynamically favored at a potential slightly below that of bulk deposition known as surface limited redox replacement (SLRR) for Pt monolayer synthesis.[21–23] Depositions of single MLs of Pt and Pd, reported by Brankovic et al., were some of the first examples of electrochemical monolayer deposition by replacing a sacrificial template of Cu.[24] This technique has been further explored as a method of layer-by-layer growth by Stickney et al. and Dimitrov et al. using Cu and Pb sacrificial layers.[25–29] The SLRR method typically involves the repeated process of electrodeposition of one sacrificial atomic monolayer, oftentimes via underpotential deposition (UPD) and its replacement by a second element via redox galvanic replacement.[30–32]

By using surface-sensitive characterization methods of X-ray photoelectron spectroscopy (XPS) and cyclic voltammetry (CV) in conjunction with the element-specific local atomic structural probe of extended X-ray absorption fine structure (EXAFS) spectroscopy, we can observe the atomic and electronic structure of the Pt overlayer as it evolves with increasing monolayer coverage. By using the oxygen reduction reaction (ORR), we are able to use the activity for a ubiquitous

electrocatalytic reaction as a probe of the near-surface effects of structure, strain, and charge transfer.

Incorporation of graphene at the interface between Pt and Au is expected to give a versatile tunability of electronic configuration and mechanical strain which will affect the binding energy of surface electrons. The presented study provides a systematic examination of the growth mechanism of Pt monolayers on graphene, along with strain induced at the interface between Pt and Au and the direct impact on the electrochemical catalytic activity.

■ RESULTS AND DISCUSSION

Sample Preparation. In this study, Pt monolayers are synthesized on Au (111) thin films supported on glass substrates. In order to examine the effects of graphene, two sample sets were synthesized. The first sample set had Pt overlayers directly deposited via SLRR on top of the Au. The second set consists of having monolayer graphene first transferred onto the Au/glass followed by the SLRR growth of Pt overlayers. These sets will be referred to as "Pt/Au" and "Pt/GR/Au" samples, respectively. A schematic of these designs are shown in Figure 1. Graphene was transferred to the Pt/GR/Au samples using a method similar to the works of Reina et al. and Yu et al.[33,34]

Platinum monolayers were grown by SLRR using UPD Cu as a sacrificial metal—a method supported by several fundamental studies.[35,36] By repeatedly replacing underpotentially deposited Cu layers with Pt through galvanic replacement, well-wetted Pt overlayers can be grown with a high level of precision. This growth method not only greatly reduces the Pt loading as compared to bulk potentiostatic Pt growth but also provides high dispersion of Pt. Each Cu deposition onto Au has previously been shown to result in approximately two-thirds of a monolayer of Cu.[21] For Pt/GR/Au samples, Cu is expected to form relatively large separated clusters with low island density.[12,37] When replaced by Pt, each iteration of the SLRR process is expected to result in a one-third monolayer of Pt of the surface as each $Pt^{4+} \rightarrow Pt$ reduction converts two Cu atoms to Cu^{2+} ions.[21] A total of ten sample configurations were prepared for this study: 1, 2, 3, 4, and 5 monolayer (ML) thick surfaces for both Pt/GR/Au samples and Pt/Au samples. Although the sample synthesis method is the same for each sample type, for samples on graphene specifically, as we do not assume full Pt wetting at all times. In order to denote differences in assumed overlayer formation between the sample sets, these Pt/GR/Au samples will be referred to as "monolayer equivalent" (ML-eq) rather than pure monolayers.

Cyclic Voltammetry. The Pt surface coverage of samples was examined via cyclic voltammetry (CV). Voltammograms were conducted in N_2-saturated 0.1 M H_2SO_4 by sweeping from 0 to 1.2 V at a scan rate of 20 mV/s. The results for 2, 3, 4, and 5 MLs for both sample sets can be seen in Figure 2. CV is a surface-sensitive technique, as currents seen are generated
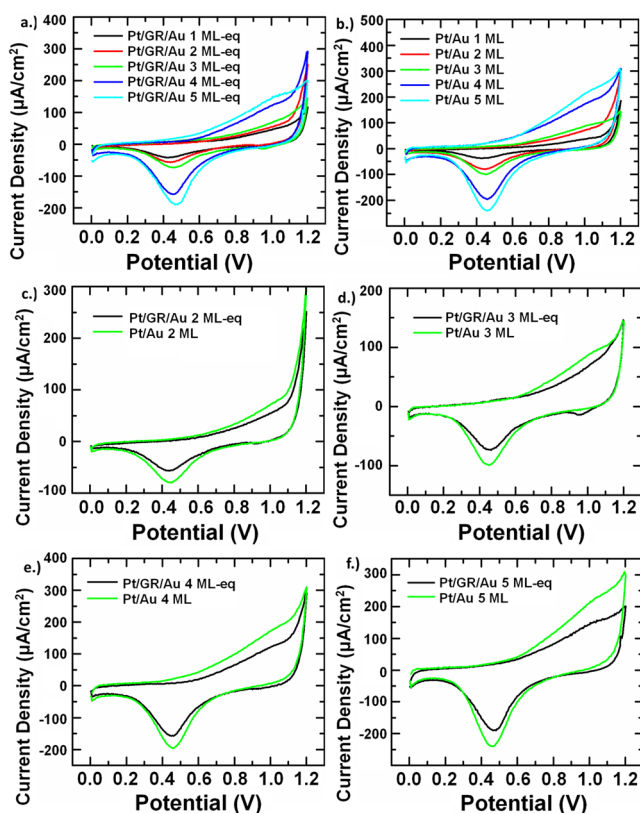
Figure 2. Cyclic voltammograms for (a) Pt/Au samples, (b) Pt/GR/Au samples, (c–f) 2, 3, 4, and 5 ML samples, respectively, comparing samples with graphene to those without. CVs were performed in N_2-saturated 0.1 M H_2SO_4. Voltages are referenced to a Ag/AgCl electrode.

from reactions at the metal–electrolyte interface. Thus, the Pt surface area can be tracked by studying the Pt oxide reduction feature at 0.45 V against Ag/AgCl reference electrode.[21] Similarly, the presence of a small Au reduction feature at 0.9 V indicates when Pt deposits are not fully masking the underlying Au. This method of tracking Pt coverage on Au has been employed successfully in the past.[21,38,39]

From Figure 2a and b, it is clear that the total surface coverage of Pt increases with SLRR iterations in both sample cases. Figure 2c–f shows that Pt/GR/Au consistently exhibits a smaller Pt oxide reduction current density when compared to Pt/Au. A small Au reduction peak is seen around 0.95 V for 2 and 3 ML-eq Pt/GR/Au samples. This is likely due to the sacrificial Cu layer clustering upon initial deposition and leaving exposed Au in patches on the surface, as mentioned by Liu et al.[12,37] For the Pt/GR/Au samples, a slight increase in the Au feature is seen from 2 to 3 ML-eq despite a larger Pt reduction feature. This indicates a further tendency of contraction or clustering of Pt atoms rather than its wetting over Au. Beginning at 4 ML-eq in the Pt/GR/Au case, the Au reduction peak disappears in CV, which indicates an eventual total coverage of Pt over graphene. This observation proves that an ultrathin layer of Pt at 4 ML-eq (1–2 nm thick) was able to fully mask the graphene/Au substrate. To our knowledge, this is the first reported full coverage of a metal on graphene at such low dimension over macroscopic surfaces areas. Pt/Au do not exhibit a Au reduction peak in CV even at 1 ML, which indicates that the Au must be fully masked by a wetted Pt layer by the first monolayer.

CVs of submonolayer coverages of Pt were also taken for each sample case, and can be seen in Figure S1 of the Supporting Information. For both Pt/Au and Pt/GR/Au, having undergone only a single SLRR iteration (nominally 0.33 MLs of Pt), we see a clear Au reduction feature. This shows that the Pt overlayer insufficiently covers the surface of the substrate and that the presence of Au can be seen when exposed to solution. We have verification, therefore, that the absence of a Au reduction feature is indicative of a fully wetted Pt overlayer at 1 ML coverage.

X-ray Photoelectron Spectroscopy. In addition to characterization by cyclic voltammetry, synthesized samples were also examined using XPS in order to determine the chemical state of the overlayer. In Figure 3, Pt is represented as
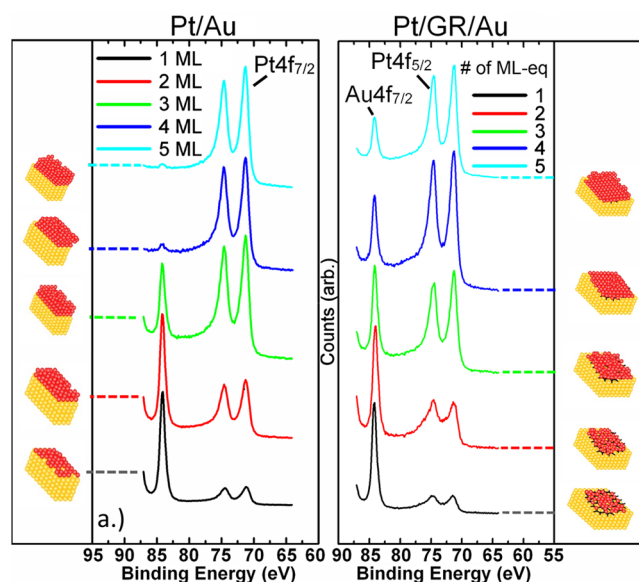

Figure 3. X-ray photoelectron spectra of Pt $4f_{7/2}$, Pt $4f_{5/2}$, and Au $4f_{7/2}$, sequentially shown from low to high binding energy, for (a) 1, 2, 3, 4, and 5 ML Pt/Au samples and (b) 1, 2, 3, 4, and 5 ML-eq Pt/GR/Au samples. Sidebars show expected sample architecture of grown Pt overlayers.

a 4f electron doublet ($4f_{7/2,5/2}$) at ∼71 and ∼74 eV, while the Au $4f_{7/2}$ photoemission is seen at ∼84 eV.[40] Due to the surface sensitive nature of electron photoemissions, the relative peak size of the Pt $4f_{7/2}$ photoemission to that of the Au $4f_{7/2}$ photoemission is related to the average thickness of the surface shell. Figure 3 shows that, for both sample cases, Pt $4f_{7/2}$ grows in intensity relative to the Au $4f_{7/2}$ when more Pt monolayers are deposited on the surface.

However, the intensity increase is not growing at the same rate between the two sample sets. When comparing the 4 and 5 ML samples, the Au photoemission is almost completely masked for Pt/Au. This indicates that there are very few core electrons from Au that are emitted beyond the top few nanometers of the surface. For the Pt/GR/Au samples, the Au photoemission is not fully diminished even at 5 ML-eq This indicates that more Au is near the surface allowing its bound electrons to be detected. This could be due to a relatively thinner Pt overlayer in some regions that allow more Au 4f electrons through than in the graphene-free case. The peak area between Pt and Au comparisons were made via peak fitting using a Shirley background and are shown in Figure 4.
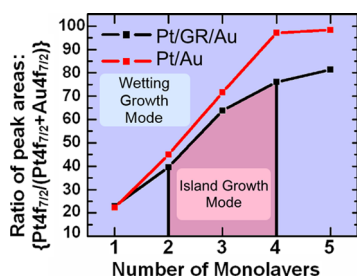
Figure 4. Representation of Pt to Au ratio by comparing the $4f_{7/2}$ peak area of Pt to the total $4f_{7/2}$ peak area of both Pt and Au as a percentage.

Figure 5. (a) EXAFS spectra for Pt/GR/Au samples of 1, 3, and 5 ML-eq and a Pt foil reference. (inset) Corresponding k-space data. (b) Schematic of Pt atoms on graphene.

Both the CV and XPS results show that growth process is not identical between the two sample cases. Cyclic voltammograms (Figure 2) show exposed Au on the surface for low monolayer Pt/GR/Au samples. XPS results cannot give an indication of surface wetting, but the data show lower average Pt thickness in the core−shell structure for the Pt/GR/Au samples as evidenced by a less intense Pt photoemission relative to Au. This supports the findings of Liu et al., which expected Cu to form more clustered structures on top of graphene, as SLRR in our case was by depositing Cu first which was replaced galvanically afterward by Pt. The sidebars in Figure 3 represent the expected surface architecture for our sample set. We surmise these representations for our samples based on the data achieved and the conclusions made by Liu et al. and Dai et al.[12,13]

Figure 4 represents the Pt $4f_{7/2}$ peak area normalized to the Au $4f_{7/2}$ peak areas. It can be seen that Pt/Au samples exhibit a larger relative Pt area and that the difference becomes more pronounced at 4 and 5 MLs. The deviation can be explained in the following way: at 3 ML-eq, the Pt/GR/Au sample undergoes Pt redistribution such that the Au substrate is re-exposed. At 4 ML-eq, the subsequent Pt deposited covers the exposed Au. Thus, while the Pt in Pt/Au continues iterative growth that results in a pseudolinear increase the ratio of Pt to Au peaks in XPS between 3 and 4 ML, the Pt in Pt/GR/Au deviates from this linearity because of the exposure and subsequent masking of Au from 3 to 4 ML-eq. The re-exposure of Au between 2 and 4 ML-eq in Pt/GR/Au necessarily implies clustering of Pt. In Figure 4 this region is denoted as the "island growth mode" for Pt/GR/Au. Only once the islands reach a threshold size at 4 ML-eq is a fully wetted layer achieved again, evidenced by lack of a Au oxide reduction peak in CV (Figure 2).

X-ray Absorption Spectroscopy. The local atomic structure around an average Pt atom was investigated using EXAFS for Pt adlayers in a subset of the Pt/GR/Au samples. In Figure 5a, we see the R-space spectra for Pt/GR/Au samples as well as for Pt foil. The y-axis in the plot is proportional to a weighted partial radial distribution function around an average Pt atom. Bulk Pt (Pt foil) exhibits an apparent nearest neighbor (nn) distance of about 2.2 Å, consistent with previous work,[21] which is actually at a Pt−Pt bond distance of 2.78 Å when corrected for the phase shifts of the electron waves in XAS. In Figure 5a we see that the 1 ML-eq sample exhibits the nn distance of bulk Pt. This is interesting because, based on the preference of Pt to adsorb onto the bridge sites of graphene.[13,15] A flat, close-packed, Pt layer arrived at by populating every other bridge site with a Pt atom (Figure 5b), would exhibit a Pt−Pt nn distance of 2.14 Å instead of the 2.78
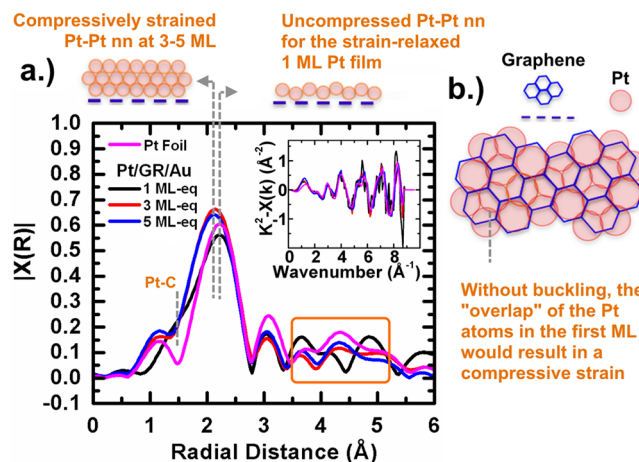
Å (phase shift corrected) nn distance we observe. At a 2.14 Å nn distance, the 1 ML-eq Pt film would under a large compressive strain (Figure 5b).We propose, instead, that this 1 ML-eq Pt film utilizes its degrees of freedom normal to the film plane to buckle, alternately adjusting the Pt-bridge distances and arriving at the 2.78 Å nn average bond length for Pt−Pt (schematically shown in Figure 5a).

The structural similarity between the buckled 1 ML-eq Pt/GR/Au Pt film and the bulk 3D structure of Pt foil is mainly restricted to the Pt−Pt nn bond. The 1 ML-eq Pt film shows a Pt−C peak shoulder at about 1.5 Å, due to its bond with graphene, which is obviously absent in the Pt foil. Furthermore, the long-range order of bonding is quite different in comparison, highlighted by the window in the observed 3.5 to 5.5 Å range Figure 5a. In this R range, the spectra for the reference foil, the nominally 3 ML-eq, and 5 ML-eq samples all line up peak for peak, but the 1 ML-eq case shows a variant long-range order. With only a single layer of Pt atoms, 1 ML-eq film does not have an evolved long-range structure resembling that of bulk Pt.

When the Pt overlayer is several monolayers thick and distanced from the underlying graphene sheet, the atoms reject the buckled template of the 1 ML-eq film and instead choose a strained face centered cubic (FCC) structure. While the 3 ML-eq and 5 ML-eq samples exhibit Pt FCC configuration, they however show a ∼ 0.1 Å (or about 3.5%) compressive strain in the nn bond. This aligns with previous observations in CV where the Au reduction peak increased at 3 ML-eq Pt atoms were subjected to more compressive stresses, increasing the exposed Au surface as a consequence. Beyond 3 ML-eq, further addition of Pt retains the compressive stress achieved at the 3 ML-eq stage, but additional Pt begin to fill in the exposed Au spots and maintain a full mask of Pt over graphene, as indicated by CV in Figure 2.

Figure S4 of the Supporting Information shows preliminary modeling for Pt atoms on a graphene support. Simple models were made for 1 ML Pt on graphene, 3 ML Pt on graphene, and bulk Pt. The 1 ML Pt/GR model is unstrained and exhibits 6-fold Pt−Pt coordination and 3-fold Pt−C coordination, representing the average Pt environment for this case. The 3 ML Pt/GR structure incorporates 3.5% compressive strain to the Pt−Pt bond, and Pt−Pt coordination is adjusted to account for the undercoordinated top and bottom layers while Pt−C

coordination is added to the bottom layer. A bulk Pt model (12-fold coordination, without strain) is also placed for comparison. We observe that the positions of the peaks in the models correspond well to the trends observed experimentally, validating the earlier conclusions on the observed compressive strain.

By introducing graphene as a sandwich layer, therefore, we have effectively created a new Pt-based species, one that has the electronic configuration and atomic structure of bulk Pt, but with higher electron density than due to its inherent compressive strain.

Catalyst Performance. When we look closer at the Pt photoemission binding energies in XPS, we see opposing trends emerging between the two sample sets, shown in Figure 6.
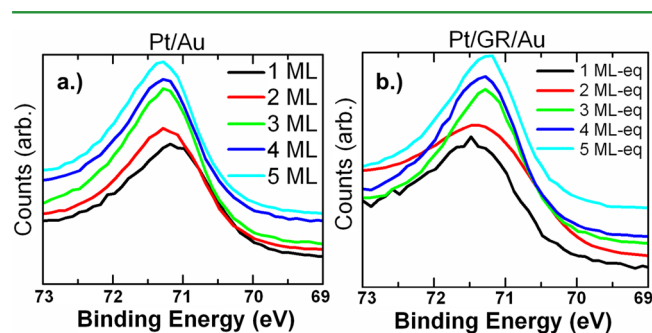

Figure 6. Pt 4f7/2 photoemission from XPS for (a) Pt/Au samples and (b) Pt/GR/Au.

For Pt/Au samples, the binding energy shifts higher, from ~71.1 to 71.3 eV, with increasing overlayer thickness. This trend has been attributed to low-dimensional electron transfer effects from Au.[20] The Au substrate transfers charge to the adsorbed Pt, an effect which diminishes with increasing Pt overlayer thickness. Pt/GR/Au samples instead show a shift to lower binding energy, from 71.3 to 71.2 eV. These results are also shown in Figure 8. We explore next whether these observed shifts in electron binding energy directly influences catalyst performance.

Electrocatalytic activity tests were conducted by performing linear sweep voltammetry (LSV), in oxygen-saturated 0.1 M H_2SO_4 at room temperature, from 0.8 to −0.1 V, in order to analyze the ORR.[41] The experimental results for each sample are shown in Figure 7. By following the first derivative peak of the ORR polarization curves, we measure the overpotential needed to catalyze the reaction. Because we sweep negatively, a higher reported potential denotes a lower required overpotential for the ORR. In order to make a comparison between the two sample cases, the Pt reduction shape in Figure 2 was used to normalize the ORR current densities with the relative amount of Pt present on the surface. Those results are shown in Figure 7, with potentials reported against Ag/AgCl reference electrodes. These results compare favorably to other studies utilizing a similar method of evaluation.[42]

Figure 7 shows that for both sample cases, increasing the number of Pt monolayers results in higher potential values for the inflection point. For the 2 and 3 ML cases, the Pt/Au showed a notably higher ORR potential compared to Pt/GR/Au samples. However, for the 4 and 5 ML cases, the inverse is observed, where Pt/GR/Au samples show higher potentials when compared to Pt/Au samples. In terms of overpotential, the Pt/GR/Au samples demonstrate appreciably lower over-
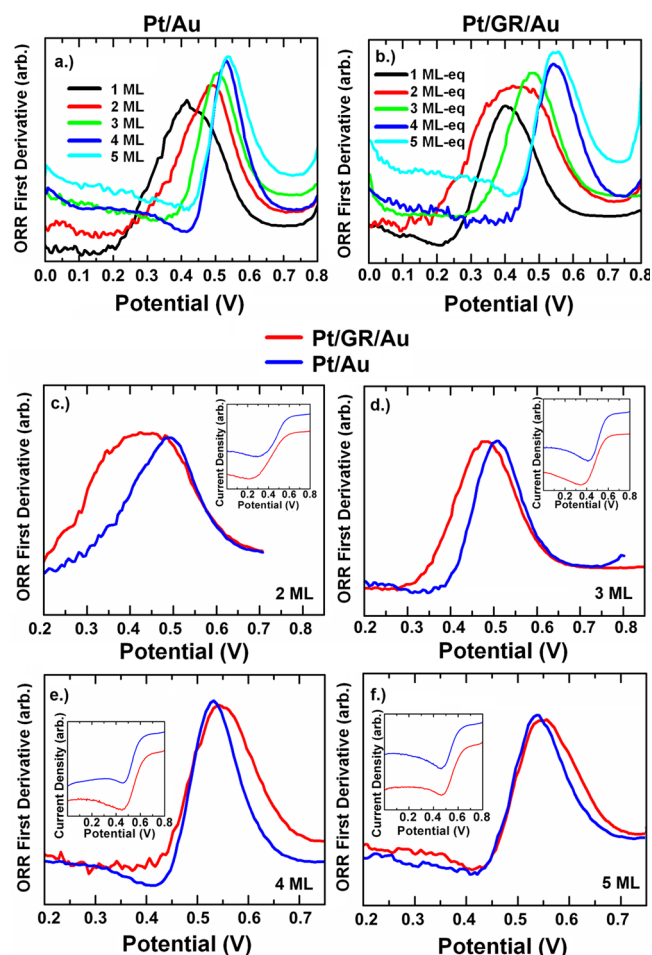
Figure 7. First derivative of oxygen reduction reaction polarization curves (against a Ag/AgCl reference electrode) obtained by linear sweep voltammetry in O^2-saturated 0.1 M H_2SO_4. (a) Pt/Au samples. (b) Pt/GR/Au samples. (c−f.) 2, 3, 4, and 5 ML, respectively. (insets) ORR polarization curves for each sample pair. The sweep rate is 20 mV/s. These curves have been normalized by the Pt surface charge obtained from the CV curves in Figure 2.

potential required once a sufficient amount of Pt is achieved on the surface. This correlates well with the binding energy values recorded, and a comparison between these experiments can be seen in Figure 8.

We see a convergence and eventual crossover of the ORR potential, as indicated by the polarization curve inflection points. This is represented in Figure 8a. Additionally, as seen earlier in Figure 6, we see opposite trends in binding energy between the two sample cases (Figure 8b). In Pt/Au samples, the low-dimensionality of the Pt overlayer allows charge transfer from the underlying Au, causing a negative shift of the core electron binding energy of the Pt monolayers. Our data shows a correlation between a negatively shifted binding energy and a diminished ORR potential for these samples. This correlation can be explained by the adsorption of OH− groups on Pt surface. Adzic et al. have reported how desorption of OH− species from the catalyst surface is a crucial process in allowing completion of the electronic reduction of O_2 to H_2O.[18] Previous research has shown that OH− species on the surface of a Pt shell less than two MLs thick require more energy to be removed than from a bulk Pt surface.[20] This supports the ORR observations here for the present sample set,
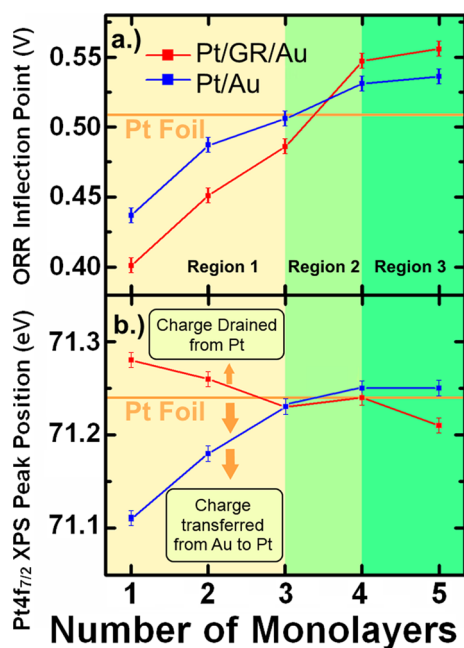
Figure 8. (a) Inflection point of the ORR polarization curves and (b) the Pt $4f_{7/2}$ photoemission binding energy for each sample case. A horizontal line is used to reference the binding energy of bulk Pt foil. Region 1 is explained by charge transfer mechanisms, from Au to Pt in the case of Pt/Au samples, and from Pt to graphene in the Pt/GR/Au case. Region 2 shows where charge transfer mechanisms have significantly diminished into Region 3, where graphene interfacial strain is lowering the binding energy of the Pt overlayer and ORR overpotential surpasses that of bulk Pt.

where the ORR potential is lowered due to an increased Pt−OH adsorption. This conclusion also matches well with other studies done with similar Pt catalysts.[38] As the overlayer thickness grows, this low-dimensional effect diminishes, resulting in a binding energy which increases to that of bulk Pt as the net charge transfer approaches zero.

In Pt/GR/Au samples, Pt overlayers of low ML thickness exhibit increased binding energies in comparison to Pt/Au. This is seen in Region 1 of Figure 8. This binding energy increase can be explained by surface charge calculations for noble metals adsorbed on graphene. Thermodynamically, Pt favors adsorbing on the graphene at the bridge site between two C atoms, as mentioned earlier when discussing our EXAFS data. A Pt atom forms a polarized covalent bond with the C atoms underneath, and pushes them to move apart from one another. This bonding has been calculated to lower the charge of the adsorbed Pt by 0.108 electrons.[43] With this diminished surface charge, we expect the binding energy of Pt photoemissions in XPS to be slightly increased as the data shows.

The XPS data indicates that this electron donation from Pt to graphene is diminished with increasing monolayer thickness, and the binding energy decreases to that of bulk Pt foil. Assuming that the unoccupied densities of states in graphene is already saturated by the available electron density from 1 ML of Pt, any additional Pt deposited will diminish the share of electron density transferred to graphene per Pt adatom. Thus, for the Pt/GR/Au sample set, the binding energy of Pt electrons diminishes as the overlayer thickness grows. The binding energies of the two sample sets converge at 3 ML. We also see the convergence of the overpotential point between 3 and 4 ML. These two phenomena are represented by the

Region 2. The Pt is no longer donating any electron density once it achieves 4 ML-eq in thickness but is still affected by partially strained early monolayers, which causes a lattice mismatch resulting in increasing the ORR potential.

The 4 and 5 ML samples for both Pt/GR/Au and Pt/Au cases show lower ORR overpotential than bulk Pt foil, as observed in Region 3. The monolayer-scale platinum surface exhibits a higher percentage of close-packed Pt in comparison to that of bulk polycrystalline Pt, resulting from pseudoepitaxial growth over the respective Au (111) and graphene substrates. The lower the amount of imperfections and the more ordered the Pt surface, the better it can be active toward ORR due to weaker OH− binding. Both our monolayer architectures can be expected to be more ordered and more defect free than Pt foil. Thanks to a compressed overlayer, as inferred from EXAFS data, it is also clear that 4 and 5 ML-eq Pt/GR/Au samples achieve an additional boost in catalytic aptitude. This strain, caused by the graphene, will cause a decrease of the Pt−OH adsorption energy, further reducing the coverage of OH− species on the surface that inhibit the oxygen reduction.[17]

Catalyst Durability. One of the major requirements for an effective catalyst is its durability. Earlier efforts looked to using carbon support materials, such as carbon black, in order to enhance Pt retention.[44] While some improvement of catalytic activity was achieved, the durability of Pt catalysts remains a critical issue. Graphene has already been shown to improve catalyst durability in a variety of configurations.[45−47] We investigated the durability of our synthesized graphene supported Pt ML catalysts by cycling in acidic media.

Samples were cycled long-term from 0.4 to 0.75 V in oxygen-saturated 0.1 M H_2SO_4, with a total of 1000 cycles performed on each sample. A characterization CV curve from 0 to 1.20 V was taken in nitrogen-saturated 0.1 M H_2SO_4, once before cycling and once after 1000 cycles in order to examine the changes in the Pt reduction shape. By measuring the integrated Pt reduction charge before and after cycling, we can obtain an illustrative representation of the amount of surface coverage of Pt remaining on these samples. This is shown in Figure 9,
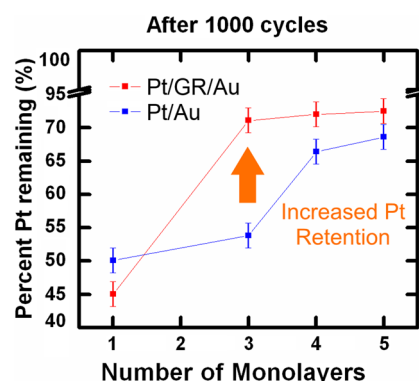
Figure 9. Using the Pt reduction shape in CV, the percentage of surface Pt is calculated after 1000 cycles in acidic media. Cycles were performed from 0.4 to 0.75 V in O^2-saturated H_2SO_4.

where total Pt retention is displayed as a percentage its original integrated area. The calculated integrated charge density values can be found in Table S1 in the Supporting Information.

For the 1 ML-eq Pt/GR/Au sample, the Pt reduction curve reduces more than 50% after 1000 cycles, showing low durability for the overlayer and is consistent with previous Pt monolayer experiments. This could be due to the unevolved

metallic bonding of the 1 ML Pt film. The 3, 4, and 5 ML-eq Pt/GR/Au samples retain Pt much more strongly than 1 ML-eq, although there is still about a ~25% loss in electrochemically active surface area after 1000 cycles.

Pt/Au samples were examined in the same fashion. The 1 ML sample showed improved retention over its Pt/GR/Au counterpart, although it achieves only 50% retention after 1000 cycles. The advantage could be due to better wetting of the initial overlayer. One monolayer Pt/Gr/Au is buckled and should have poorer adherence to GR/Au than its 1 ML Pt/Au counterpart. Four and 5 ML Pt/Au samples showed improved Pt retention but remain lower than the corresponding Pt/GR/Au samples. For the 4 and 5 ML cases, Pt/GR/Au showed improved Pt retention relative to Pt/Au with the largest difference (of about 20%) for the 3 ML case. The results indicate that loss of Pt is dictated mostly by bonding to other Pt atoms, an effect which is seemingly amplified on the graphene templated Pt due to the compressive strain. Further future work is planned to elucidate the mechanistic details of the enhanced Pt retention.

CONCLUSION

This study embodies a systematic examination on the effects of graphene when incorporated into core–shell Pt monolayer catalysts. We have grown for the first time (to the best of our knowledge) a fully wetted ultrathin layer of a metal over graphene that is nominally 4 monolayers (less than 2 nm) thick. At such low dimensions, we approach the theoretical limits of Pt loading, thereby significantly increasing the activity per Pt atom. Moreover, due to a compressive strain of the Pt surface of about 3.5%, we see an observable increase of the catalytic activity of this low-dimensional Pt relative to its bulk counterpart due to the compression from its graphene templated growth. In addition, samples seated on graphene have shown a higher Pt retention than those without, when subjected to long-term cycling experiments. The ability to induce strain on ultrathin Pt deposits, regardless of the nature of the substrate underneath, is an important new paradigm. Our research shows that by incorporating graphene as a template at metal–metal interfaces, new research opportunities can be explored in strain-tuned surface electronic properties.

EXPERIMENTAL SECTION

Individual monolayers of graphene were obtained from American Chemicals Supplier, previously synthesized by chemical vapor deposition over 25 μm Cu foil.[48] Glass substrates were cleaned in Piranha solution (H_2SO_4: H_2O_2 4:1) for 15 min, followed by physical vapor deposition of a 15 nm Cr layer and a 50 nm Au layer, successively, using Denton Explorer E-beam Evaporator. A slow deposition rate of 0.5 Å/s was used in order to achieve to most uniform Au coating possible. AFM measurements of deposited Au on glass substrates show a surface roughness value of less than 1 nm (RMS). XRD analysis shows that the deposited Au surface is largely of a (111) orientation and can be seen in Figure S3 of the Supporting Information. The chromium acts as an adhesion layer for the Au, which acts as our core metal.

For Pt/GR/Au samples, a 100 nm thick PMMA (poly(methyl methacrylate)) layer was spin coated over graphene/Cu foil and left overnight to dry. The underlying Cu foil was then etched away by floating on nitric acid, with the coated PMMA layer facing up, followed by floating overnight in an ammonium persulfate solution. This was succeeded by cleaning in 18.2 MΩ deionized water bath and isopropyl alcohol.[49] After etching, the PMMA/graphene film was then transferred over to the Au substrate. The PMMA/graphene/substrate was then baked at 220 °C for 15 min with a ramp up from room temperature at 20 °C/min. After baking, the substrate was placed in acetone to etch away the PMMA for 8 h.

Once the substrate was ready for Pt deposition, Cu UPD was used to grow a sacrificial layer followed by galvanic replacement of Pt. By stopping the voltage sweep at a potential between the bulk removal and the UPD removal potentials for Cu, the surface coverage of the Cu UPD layer is self-limiting. See Figure S2 in the Supporting Information for representative Cu UPD voltammograms for both Pt/Au and Pt/GR/Au samples. The resulting Cu surface was then galvanically replaced by Pt atoms from solution. SLRR procedure was repeated to grow the Pt overlayer with monolayer-scale precision. All synthesis was done at room temperature in a glass cell with a hanging meniscus arrangement. All solutions used were deaerated by bubbling with ultrahigh purity nitrogen before any chemical processes. Any potentials are reported relative to homemade Ag/AgCl reference electrodes. Pt wire was used for the counterelectrodes. The solution used for Cu UPD was 10 mM $CuSO_4$ + 50 mM H_2SO_4 and Pt galvanic replacement of the Cu utilized 1 mM H_2PtCl_6.

The core-level electronic structure of the samples was examined by (XPS) via a Thermo K-Alpha XPS system using an Al Kα source. Cyclic voltammetry was employed to evaluate the surface coverage of Pt. EXAFS spectra at the Pt L3 edge was obtain at Brookhaven National Lab's National Synchrotron Light Source beamline X3B. Data was collected in fluorescence mode using a 13 element solid state detector. Data handling for EXAFS was done using the ATHENA package. Linear sweep voltammetry was used to observe the sample surface activity by probing the oxygen reduction reaction. Finally, surface durability was examined via cycling tests in sulfuric acid. All potentials reported here are relative to homemade Ag/AgCl reference electrodes.

ASSOCIATED CONTENT

⑤ Supporting Information

Includes cyclic voltammograms of submonolayer Pt coverage samples, cyclic voltammograms for Cu UPD step in SLRR, integrated charge densities used for Pt retention analysis, XRD spectra for the Au substrate, and simple EXAFs models for Pt and C bond analysis. This material is available free of charge via the Internet at http://pubs.acs.org.

AUTHOR INFORMATION

Corresponding Author

*E-mail: faisal.alamgir@mse.gatech.edu.

Author Contributions

†A.A. and A.V. contributed equally.

Notes

The authors declare no competing financial interest.

REFERENCES

(1) Kim, K.; Choi, J. Y.; Kim, T.; Cho, S. H.; Chung, H. J. A Role for Graphene in Silicon-based Semiconductor Devices. *Nature* **2011**, *479*, 338−344.

(2) Venugopal, A.; Colombo, L.; Vogel, E. M. Contact Resistance in Few and Multilayer Graphene Devices. *Appl. Phys. Lett.* **2010**, *96*, 013512.

(3) Lee, E. J. H.; Balasubramanian, K.; Weitz, R. T.; Burghard, M.; Kern, K. Contact and Edge Effects in Graphene Devices. *Nat. Nanotechnol.* **2008**, *3*, 486−490.

(4) Wang, D.; Xin, H. L.; Hovden, R.; Wang, H.; Yu, Y.; Muller, D. A.; DiSalvo, F. J.; Abruña, H. D. Structurally Ordered Intermetallic Platinum-cobalt Core-shell Nanoparticles with Enhanced Activity and Stability as Oxygen Reduction Electrocatalysts. *Nat. Mater.* **2013**, *12*, 81−87.

(5) Gong, W.; Zhang, W.; Ren, C.; Ke, X.; Wang, S.; Huai, P.; Zhang, W.; Zhu, Z. Strain-controlled Interface Engineering of Binding and Charge Doping at Metal-graphene Contacts. *Appl. Phys. Lett.* **2013**, *103*, 143107.

(6) Mavrikakis, M.; Hammer, B.; Norskov, J. K. Effect of Strain on the Reactivity of Metal Surfaces. *Phys. Rev. Lett.* **1998**, *81*, 2819−2822.

(7) Gong, C.; Hinojos, D.; Wang, W. C.; Nijem, N.; Shan, B.; Wallace, R. M.; Cho, K. J.; Chabal, Y. J. Metal-Graphene-Metal Sandwich Contacts for Enhanced Interface Bonding and Work Function Control. *ACS Nano* **2012**, *6*, 5381−5387.

(8) Li, Y. M.; Tang, L. H.; Li, J. H. Preparation and Electrochemical Performance for Methanol Oxidation of Pt/graphene Nanocomposites. *Electrochem. Commun.* **2009**, *11*, 846−849.

(9) Shang, N. G.; Papakonstantinou, P.; Wang, P.; Ravi, S.; Silva, P. Platinum Integrated Graphene for Methanol Fuel Cells. *J. Phys. Chem. C* **2010**, *114*, 15837−15841.

(10) Hammer, B.; Norskov, J. K. Theoretical Surface Science and Catalysis - Calculations and Concepts. *Adv. Catal.* **2000**, *45*, 71−129.

(11) Pedersen, M. O.; Helveg, S.; Ruban, A.; Stensgaard, I.; Laegsgaard, E.; Norskov, J. K.; Besenbacher, F. How a Gold Substrate can Increase the Reactivity of a Pt Overlayer. *Surf. Sci.* **1999**, *426*, 395−409.

(12) Liu, X.; Wang, C.-Z.; Hupalo, M.; Lin, H.-Q.; Ho, K.-M.; Tringides, M. Metals on Graphene: Correlation Between Adatom Adsorption Behavior and Growth Morphology. *Phys. Chem. Chem. Phys.* **2012**, *14*, 9157−9166.

(13) Dai, X. Q.; Tang, Y. N.; Zhao, J. H.; Dai, Y. W. Absorption of Pt Clusters and the Induced Magnetic Properties of Graphene. *J. Phys.: Condens. Matter* **2010**, *22*, 316005.

(14) Chan, K. T.; Neaton, J. B.; Cohen, M. L. First-principles Study of Metal Adatom Adsorption on Graphene. *Phys. Rev. B* **2008**, *77*, 235430.

(15) He, H. K.; Gao, C. Graphene Nanosheets Decorated with Pd, Pt, Au, and Ag Nanoparticles: Synthesis, Characterization, and Catalysis Applications. *Sci. China: Chem.* **2011**, *54*, 397−404.

(16) Sun, S. H.; Zhang, G. X.; Gauquelin, N.; Chen, N.; Zhou, J. G.; Yang, S. L.; Chen, W. F.; Meng, X. B.; Geng, D. S.; Banis, M. N.; Li, R. Y.; Ye, S. Y.; Knights, S.; Botton, G. A.; Sham, T. K.; Sun, X. L. Single-atom Catalysis Using Pt/Graphene Achieved through Atomic Layer Deposition. *Sci. Rep.* **2013**, *3*, 1775.

(17) Adzic, R. Platinum Monolayer Electrocatalysts: Tunable Activity, Stability, and Self-Healing Properties. *Electrocatalysis* **2012**, *3*, 163−169.

(18) Adzic, R. R.; Zhang, J.; Sasaki, K.; Vukmirovic, M. B.; Shao, M.; Wang, J. X.; Nilekar, A. U.; Mavrikakis, M.; Valerio, J. A.; Uribe, F. Platinum monolayer Fuel Cell Electrocatalysts. *Top. Catal.* **2007**, *46*, 249−262.

(19) Zhang, S. S.; Yuan, X. Z.; Hin, J. N. C.; Wang, H. J.; Friedrich, K. A.; Schulze, M. A Review of Platinum-based Catalyst Layer Degradation in Proton Exchange Membrane Fuel Cells. *J. Power Sources* **2009**, *194*, 588−600.

(20) Rettew, R. E.; Cheng, S.; Sauerbrey, M.; Manz, T. A.; Sholl, D. S.; Jaye, C.; Fischer, D. A.; Alamgir, F. M. Near Surface Phase Transition of Solute Derived Pt Monolayers. *Top. Catal.* **2013**, *56*, 1065−1073.

(21) Cheng, S.; Rettew, R. E.; Sauerbrey, M.; Alamgir, F. M. Architecture-Dependent Surface Chemistry for Pt Monolayers on Carbon-Supported Au. *ACS Appl. Mater. Interfaces* **2011**, *3*, 3948.

(22) Rettew, R. E.; Guthrie, J. W.; Alamgir, F. M. Layer-by-Layer Pt Growth on Polycrystalline Au: Surface-Limited Redox Replacement of Overpotentially Deposited Ni Monolayers. *J. Electrochem. Soc.* **2009**, *156*, D513−D516.

(23) Rettew, R. E.; Guthrie, J. W.; Jayeb, C.; Fischer, D.; Alamgir, F. M. Synthesis and Characterization of Monolayer Bimetallic Surfaces: A Synchrotron NEXAFS and XPS Study. *ECS Trans.* **2009**, *19*, 97−106.

(24) Gokcen, D.; Bae, S. E.; Brankovic, S. R. Stoichiometry of Pt Submonolayer Deposition via Surface-Limited Redox Replacement Reaction. *J. Electrochem. Soc.* **2001**, *157*, D582−D587.

(25) Kim, Y.; Kim, J.; Vairavapandian, D.; Stickney, J. Platinum nanofilm formation by EC-ALE via redox replacement of UPD copper: Studies using in-situ scanning tunneling microscopy. *J. Phys. Chem. B* **2006**, *110*, 17998−18006.

(26) Kim, J.; Kim, T.; Stickney, J. Cu nanofilm formation by electrochemical atomic layer deposition (ALD) in the presence of chloride ions. *J. Electroanal. Chem.* **2008**, *621*, 205−213.

(27) Thambidurai, C.; Kim, Y.; Stickney, J. Electrodeposition of Ru by atomic layer deposition (ALD). *Electrochim. Acta* **2008**, *52*, 6157−6164.

(28) Fayette, M.; Liu, Y.; Bertrand, D.; Nutariya, J.; Vasiljevic, N.; Dimitrov, N. From Au to Pt via Surface Limited Redox Replacement of Pb UPD in One-Cell Configuration. *Langmuir* **2011**, *27*, 5650−5658.

(29) Jayaraju, N.; Vairavapandian, D.; Kim, Y.; Banga, D.; Stickney, J. L. Electrochemical Atomic Layer Deposition (E-ALD) of Pt Nanofilms Using SLRR Cycles. *J. Electrochem. Soc.* **2012**, *159*, D616−D622.

(30) Leiva, E. Recent Developments in the Theory of Metal UPD. *Electrochim. Acta* **1996**, *41*, 2185−2206.

(31) Herrero, E.; Buller, L. J.; Abruna, H. D. Underpotential Deposition at Single Crystal Surfaces of Au, Pt, Ag and Other Materials. *Chem. Rev.* **2001**, *101*, 1897−1930.

(32) Gewirth, A. A.; Niece, B. K. Electrochemical Applications of in Situ Scanning Probe Microscopy. *Chem. Rev.* **1997**, *97*, 1129−1162.

(33) Reina, A.; Jia, X. T.; Ho, J.; Nezich, D.; Son, H. B.; Bulovic, V.; Dresselhaus, M. S.; Kong, J. Large Area, Few-Layer Graphene Films on Arbitrary Substrates by Chemical Vapor Deposition. *Nano Lett.* **2009**, *9*, 30−35.

(34) Yu, Q. K.; Lian, J.; Siriponglert, S.; Li, H.; Chen, Y. P.; Pei, S. S. Graphene Segregated on Ni Surfaces and Transferred to Insulators. *Appl. Phys. Lett.* **2008**, *93*, 113103.

(35) Mrozek, M. F.; Xie, Y.; Weaver, M. J. Surface-enhanced Raman Scattering on Uniform Platinum-group Overlayers: Preparation by Redox Replacement of Underpotential-deposited Metals on Gold. *Anal. Chem.* **2001**, *73*, 5953−5960.

(36) Gokcen, D.; Bae, S. E.; Brankovic, S. R. Stoichiometry of Pt Submonolayer Deposition via Surface-Limited Redox Replacement Reaction. *J. Electrochem. Soc.* **2010**, *157*, D582−D587.

(37) Liu, X.; Wang, C. Z.; Hupalo, M.; Lu, W. C.; Tringides, M. C.; Yao, Y. X.; Ho, K. M. Metals on Graphene: Correlation Between Adatom Adsorption Behavior and Growth Morphology. *Phys. Chem. Chem. Phys.* **2012**, *14*, 9157−9166.

(38) Zhai, J.; Huang, M.; Dong, S. Electrochemical Designing of Au/Pt Core Shell Nanoparticles as Nanostructured Catalyst with Tunable Activity for Oxygen Reduction. *Electroanalysis* **2007**, *19*, 506−509.

(39) Tang, H.; Chen, J. H.; Wang, M. Y.; Nie, L. H.; Kuang, Y. F.; Yao, S. Z. Controlled Synthesis of Platinum Catalysts on Au Nanoparticles and their Electrocatalytic Property for Methanol Oxidation. *Appl. Catal., A* **2004**, *275*, 43−48.

(40) Selvarani, G.; Selvaganesh, S. V.; Krishnamurthy, S.; Kiruthika, G. V. M; Sridhar, P.; Pitchumani, S.; Shukla, A. K. A Methanol-Tolerant Carbon-Supported Pt-Au Alloy Cathode Catalyst for Direct Methanol Fuel Cells and Its Evaluation by DFT. *J. Phys. Chem. C* **2009**, *113*, 7461−7468.

(41) Zignani, S. C.; Antolini, E.; Gonzalez, E. R. Evaluation of the Stability and Durability of Pt and Pt-Co/C Catalysts for Polymer Electrolyte Membrane Fuel Cells. *J. Power Sources* **2008**, *182*, 83−90.

(42) Qiu, J.-D.; Wang, G.-C.; Liang, R.-P.; Xia, X.-H.; Yu, H.-W. Controllable Deposition of Platinum Nanoparticles on Graphene as an

Electrocatalyst for Direct Methanol Fuel Cells. *J. Phys. Chem. C* **2011**, *115*, 15639−15645.

(43) Tang, Y. A.; Yang, Z. X.; Dai, X. Q. Noble Metals Induced Magnetic Properties of Graphene. *J. Magn. Magn. Mater.* **2011**, *323*, 2441−2447.

(44) Huang, C. C.; Li, C.; Shi, G. Q. Graphene Based Catalysts. *Energy Environ. Sci.* **2012**, *5*, 8848−8868.

(45) Wang, C. M.; Ma, L.; Liao, L. W.; Bai, S.; Long, R.; Zuo, M.; Xiong, Y. J. A Unique Platinum-Graphene Hybrid Structure for high Activity and Durability in Oxygen Reduction Reaction. *Sci. Rep.* **2013**, *3*, 2580.

(46) Hur, S. H.; Park, J. N. Graphene and its Application in Fuel Cell Catalysis: a Review. *Asia-Pac. J. Chem. Eng.* **2013**, *8*, 218−233.

(47) Machado, B. F.; Serp, P. Graphene-based Materials for Catalysis. *Catal. Sci. Technol.* **2012**, *2*, 54−75.

(48) Li, X. S.; Cai, W. W.; An, J. H.; Kim, S.; Nah, J.; Yang, D. X.; Piner, R.; Velamakanni, A.; Jung, I.; Tutuc, E.; Banerjee, S. K.; Colombo, L.; Ruoff, R. S. Large-Area Synthesis of High-Quality and Uniform Graphene Films on Copper Foils. *Science* **2009**, *324*, 1312−1314.

(49) Chan, J.; Venugopal, A.; Pirkle, A.; McDonnell, S.; Hinojos, D.; Magnuson, C. W.; Ruoff, R. S.; Colombo, L.; Wallace, R. M.; Vogel, E. M. Reducing Extrinsic Performance-Limiting Factors in Graphene Grown by Chemical Vapor Deposition. *ACS Nano* **2012**, *6*, 3224−3229.